Journal of Power Sources 246 (2014) 522–530

Contents lists available at ScienceDirect

Journal of Power Sources

journal homepage: www.elsevier.com/locate/jpowsour

Short communication

Fabrication of phosphotungstic acid functionalized mesoporous silica composite membrane by alternative tape-casting incorporating phase inversion technique

Li Bai [a,b], Lan Zhang [a,c,*], Hong Quan He [a,c], Raj Kamal S/O Abdul Rasheed [b,c], Cai Zhi Zhang [b,c], Ovi Lian Ding [b,c], Siew Hwa Chan [a,b,c,*]

[a] Temasek Laboratories @NTU, Nanyang Technological University, 50 Nanyang Drive, Singapore 637553, Singapore
[b] School of Mechanical and Aerospace Engineering, Nanyang Technological University, 50 Nanyang Avenue, Singapore 639798, Singapore
[c] Energy Research Institute @NTU, Nanyang Technological University, 50 Nanyang Drive, Singapore 637553, Singapore

HIGHLIGHTS

- Composite membranes have been fabricated by tape-casting & phase inversion technique.
- Such thin inorganic proton exchange membranes can be easily scaled up.
- The TGA results demonstrated that the composite membranes can operate stably below 200 °C.

ARTICLE INFO

Article history:
Received 20 May 2013
Received in revised form
24 July 2013
Accepted 31 July 2013
Available online 14 August 2013

Keywords:
Tape-casting incorporating phase inversion technique
High temperature proton exchange membrane fuel cell
Phosphotungstic acid
Meso-porous silica
Vacuum assisted wet impregnation

ABSTRACT

Meso-porous silica (MCM-41) membranes functionalized by phosphotungstic acid (HPW) for high temperature proton exchange membrane fuel cells (HT-PEMFCs) are successfully developed by a cost-effective tape-casting incorporating phase inversion and vacuum assisted wet impregnation techniques. The microstructure of the membrane is characterized by field emission scanning electron microscopy (FESEM). The effect of MCM-41 content on the tensile strength, ultimate elongation, and weight gain ratio and swelling ratio in water/methanol of the membranes are investigated in detail. The thermal stability of MCM-41 membrane with/without HPW is analyzed by thermogravimetric analysis (TGA) and derivative thermogravimetry (DTG) techniques. In particular, the effects of HPW loading and MCM-41 content on the proton conductivity of HPW/MCM-41 membranes are studied comprehensively. The results on the swelling ratio and tensile tension show that the developed membranes can be applied as an electrolyte membrane for HT-PEMFCs. The developed MCM-41 membrane, in which polyethersulfone (PESf) is used as the supporting backbone, is able to operate up to 200 °C. The single cell assembled from HPW/MCM-41 membrane with 70 wt.% HPW loading gives a peak output power of ~230 mW cm^{-2} and ~125 mW cm^{-2} in H_2/air at 90 °C and in methanol/air at 150 °C without any humidification, respectively.

1. Introduction

Proton exchange membrane fuel cells (PEMFCs) attract considerable attention to power various applications, such as, electric vehicle, domestic power generation, portable and stationary power source [1,2] due to their advantages in high-energy conversion efficiency, high power density, simplicity of operation and eco-friendly nature [3–7]. The polymer electrolyte membrane, a key component of the PEMFC, acts as both a separator and an electrolyte in the fuel cell. The membrane must satisfy a number of criterion: a) high ionic conductivity, b) zero electronic conductivity, c) high mechanical strength, d) low gas permeability, e) high cation transport number, f) mechanical and chemical stability at the operating temperature, and g) acceptable water transport characteristics. Ideally, it should also be easy and cheap to manufacture. Our technology scan in the field of polymer electrolyte for PEMFCs finds that perfluorosulphonic acid (PFSA) based Nafion membranes from DuPont Company are the de facto standard [8]. PFSA Nafion membranes offer a relatively high ionic conductivity, a cation

* Corresponding authors. Energy Research Institute @NTU, Nanyang Technological University, 50 Nanyang Drive, Singapore 637553, Singapore. Tel./fax: +65 6790 5591.
E-mail addresses: zhanglan@ntu.edu.sg (L. Zhang), mshchan@ntu.edu.sg (S.H. Chan).

0378-7753/$ – see front matter © 2013 Elsevier B.V. All rights reserved.
http://dx.doi.org/10.1016/j.jpowsour.2013.07.119

transport number near unity, zero electronic conductivity, and relatively low gas permeability [1].

It is well-known that the efficiency of PEMFCs can be further improved by increasing the operating temperature of the fuel cells up to 120 °C due to the enhanced electrodes reaction kinetics and improved CO tolerance [9,10]. However, the proton conductivity of Nafion membrane depends strongly on the water content of the membrane and decreases significantly with increasing temperature or decreasing relative humidity because of the loss of water from the membrane under conditions of high temperature or low humidities [11–13]. Therefore, the development of proton exchange membranes with high conductivity, and performance stability at high temperature and low humidity is a very critical component in this area.

Many inorganic-based proton conductors have been explored as the electrolytes for HT-PEMFCs, such as heteropoly acid (HPA)-based composite [14,15], ammonium polyphosphate (APP)-based composite [16], and doped SnP_2O_7 [17,18]. Among these solid inorganic proton conductive electrolyte materials, phosphotungstic acid ($H_3PW_{12}O_{40}$, HPW), one kind of HPAs with Keggin structure shows the highest stability and strongest acidity. Although earlier effort on this material as a potential solid electrolyte has failed to meet the requirements due to its high solubility in water and strong humidity-dependent proton conductivity [19]. In recent years, researchers have paid more attention on the immobilization of HPA. For example, Tang and co-workers reported to the use of a one-step self assembled method to immobilize the HPW molecular inside the mesoporous silica structure via a hydrogen-bond and electrostatic self-assembly assisted with a structure-directing surfactant (a non-ionic triblock copolymer $EO_{20}PO_{70}EO_{20}$) [20,21]. A fuel cell based on a 165 μm thick HPW–silica nanocomposite membrane achieved a maximum power output of 128.5 and 112.0 mW cm^{-2} for direct methanol and ethanol fuel cells, respectively, at 200 °C [20]. Lu and co-workers reported the immobilization of HPW molecules inside the mesoporous silica structure by using a novel and cost-effective vacuum-assisted wet impregnation method. And the cell fabricated from such HPW-impregnated meso-silica membrane demonstrated a peak power density of 90 mW cm^{-2} in methanol/O_2 at 150 °C and an extremely low relative humidity of 0.67% [14].

Apart from the performance of HPW/MCM-41 composite membrane, another technical challenge for such HPW-based inorganic proton conductive electrolyte relates to the feasibility of forming of thin and dense membrane structure with high mechanical strength without sintering treatment.

There are various processing techniques available for the fabrication of inorganic proton conductive composite membranes, such as die-pressing [14], casting [15], recasting [13], and cold-rolling [18]. Novel ceramic moulding technique, e.g., the water-based gel-casting has also been introduced to fabricate inorganic proton conductive composite membranes in our group recently [22]. Gel-casting is a low-cost technique commonly used in ceramic industry to fabricate complex three-dimensional ceramic parts [23], and has been successfully used to prepare components and synthesize electrode and electrolyte powders for solid oxide fuel cells (SOFCs) [24–30]. However, until now it is difficult to further decrease the thickness of the HPW functionalized mesoporous silica fabricated by gel-casting technique at the current stage. It has been reported that the cell resistance decreases with the reduction in electrolyte thickness [31], which implies that the cell performance depends on the thickness of electrolyte membrane. This means that the key contributor for the development of high performance HT-PEMFC lies in creating thin composite electrolyte membranes.

Tape casting is a well known colloidal shaping technique utilized to produce flat, and large-area ceramic tapes in a thickness range of 10–1000 μm, which can be difficult to achieve with other methods, such as pressing and extruding [32–34]. Using the tape casting technique, a pristine MCM-41 membrane has been successfully fabricated in our laboratory (see Fig. 1a). However, the chemical stability of membrane fabricated by non-aqueous based tape-casting emerges as an issue when methanol/ethanol is used as fuel. The other problem relates to the thermal stability of the membrane resulting from the thermal decomposition of organic additives ~150 °C (refer to Fig. 1b). These two technical problems serve as the motivation to develop the existing tape-casting technique to fabricate thin HPW/meso-porous silica composite membrane with good chemical and thermal stability.

In this paper, the organic–inorganic composite membranes with various mesoporous silica MCM-41 contents were fabricated by the tape-casting incorporating phase inversion techniques. The properties of MCM-41 membranes were studied by field emission scanning electron microscopy (FESEM), tensile strength test, and water/methanol uptake and swelling tests. HPW was impregnated into MCM-41 composite membranes by the method of vacuum assisted wet impregnation to enforce proton conductivity. The thermal stability of membrane with/without HPW impregnation treatment was characterized by TGA/DTG technique. The effect of MCM-41 content on the proton conductivity and single cell performance were investigated in detail.

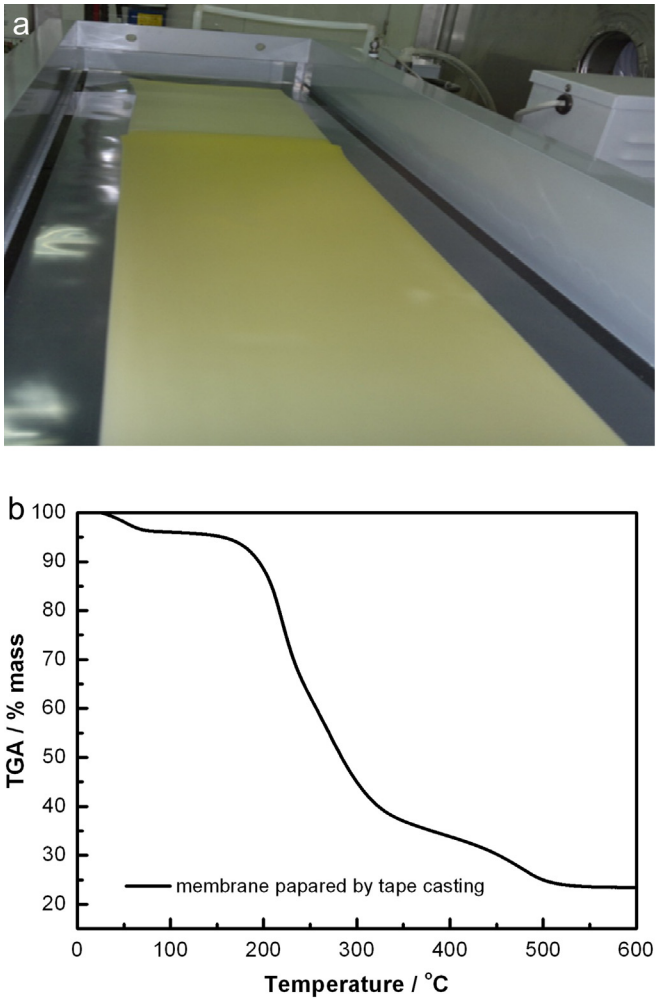

Fig. 1. (a) Optical picture of the pristine MCM-41-m membrane fabricated by tape-casting & phase inversion process, (b) thermogravimetric analysis (TGA) of this pristine membrane.

2. Experimental

2.1. MCM-41 powders synthesis

Mesoporous silica (MCM-41) powders were synthesized based on a typical hydrothermal procedure [35–37]. The NaOH (50 wt.% solution) was first mixed with deionized water, then fumed SiO_2 (particle size ~14 nm) was added to the solution while stirring at 45 °C until the SiO_2 was completely dispersed. Following this, the hexadecyltrimethylammonium bromide ($C_{19}H_{42}BrN$, CTAB) solution (prepared by dissolving CTAB in deionized water) was slowly dropped into the silica sol while stirring at 40 °C. The pH value of the solution was adjusted to 11.5 using 2 mol L^{-1} HCl solution. After continuously stirring for an additional 6 h at 40 °C, the sol mixture was then poured into a static autoclave at 100 °C for 72 h. After it cooled to room temperature, the solid product was filtrated out by a Buchner funnel, washed with deionized water, and dried at 60 °C for 24 h. The precursor was calcined in N_2 heated to 230 °C, then in air heated to 550 °C with a heating rate of 1 °C min^{-1} and dwelled at 500 °C for 10 h. In this work, all chemicals except for polyethersulfone were purchased from Sigma–Aldrich and used as-is without further purification treatment.

2.2. MCM-41 membrane fabrication

MCM-41 membranes were prepared by the tape-casting incorporating phase inversion techniques. Polyethersulfone (PESf) (Radel A-300, Deyuan Technology Co., Nanjing, China) was completely and proportionally dissolved in the *N*-methyl-2-pyrrolidone (NMP) (>99.8%) solvent using a magnetic stirrer at a rotational speed of around 500 rpm prior to usage. MCM-41 and the dispersant were then added into the PESf–NMP mixture, and ball milled for 4 h at a speed of 150 rpm to form homogenous slurry. After degassed at room temperature for 30 min, the slurry was then cast onto a clean and dry glass plate using a self fabricated casting device. The casting film was immediately immersed in tap water to solidify. After the solidification process was completed, the as-fabricated membrane was cut and dried in the oven. For simplicity purpose, all the composite membrane was named after the following general formula, *x*MCM-41–*y*HPW-m ($55 \leq x \leq 75$, $0 \leq y \leq 100$). Where "*x*" refers to the MCM-41 weight percentage in the pristine MCM-41/PESf composite membrane (see Table 1), where "*y*" refers to the weight percentage of HPW loading in the MCM-41/PESf/HPW composite membranes (see Table 2). The flow chart and schematic of tape-casting incorporating phase inversion process for the MCM-41 membrane are shown in Figs. 2 and 3, respectively.

2.3. HPW/MCM-41 composite membrane fabrication

Phosphotungstic acid (HPW) was used as the proton transport materials. HPW/MCM-41 composite membrane was prepared by a vacuum assisted impregnation method [14,22]. MCM-41 membranes were first dried in oven at 80 °C for 24 h and treated under vacuum for 0.5 h to remove moisture, impurities and trapped air inside the mesoporous structure. Then an HPW aqueous solution was added to immerse the MCM-41 membranes under vacuum. Finally, the resulting membranes were dried in oven at 80 °C for 24 h.

Table 1
Composition of MCM-41, PESf and dispersant in the pristine composite membranes.

Samples	MCM-41 (wt.%)	PESf (wt.%)	Dispersant (wt.%)
55MCM-41-m	55.00	43.56	1.44
60MCM-41-m	60.00	38.56	1.44
65MCM-41-m	65.00	33.56	1.44
70MCM-41-m	70.00	28.56	1.44
75MCM-41-m	75.00	23.56	1.44

Table 2
Composition of HPW and pristine composite membranes in the final HPW impregnated composite membranes.

Samples	Pristine MCM-41 membrane (wt.%)	HPW (wt.%)
60MCM-41–10HPW-m	90.00	10.00
60MCM-41–30HPW-m	70.00	30.00
60MCM-41–50HPW-m	50.00	50.00
60MCM-41–70HPW-m	30.00	70.00
55MCM-41–70HPW-m	30.00	70.00
65MCM-41–70HPW-m	30.00	70.00
70MCM-41–70HPW-m	30.00	70.00
75MCM-41–70HPW-m	30.00	70.00

2.4. MCM-41 powders and composite membranes characterization

Phase development of MCM-41 powders was determined by small-angle X-ray scattering (SAXS, PANalytical diffractometer, Model: Empyrean 9430.060.03002) using a Cu$K\alpha$ radiation (λ = 1.5406 Å) at 40 kV, 40 mA under room temperature. X-ray scans were run over a 2θ spectrum of 0.5°–5° at a scan rate of 0.02° s^{-1}. The morphology of the MCM-41 powder was examined by a high resolution transmission electron microscopy (TEM, JEM-2010FEF) at an acceleration voltage of 220 kV.

The scanning electron microscopy (SEM) images of the upper surface (air side, see Fig. 3), lower surface (glass plate side, see Fig. 3) and cross-section of MCM-41 membranes were investigated on a FESEM (JSM-7600F, JEOL) with an accelerating voltage of 5 kV. The surfaces of samples were coated with gold.

Tensile strength of the *x*MCM-41-m ($55 \leq x \leq 75$) membranes was measured using an Instron 5565 Universal Testing at a strain rate of 2 mm min^{-1} under ambient conditions. The gauge length and width of dumbbell specimens were 40 mm and 10 mm, respectively. At least nine measurements were conducted for each membrane, and the average values were calculated for the

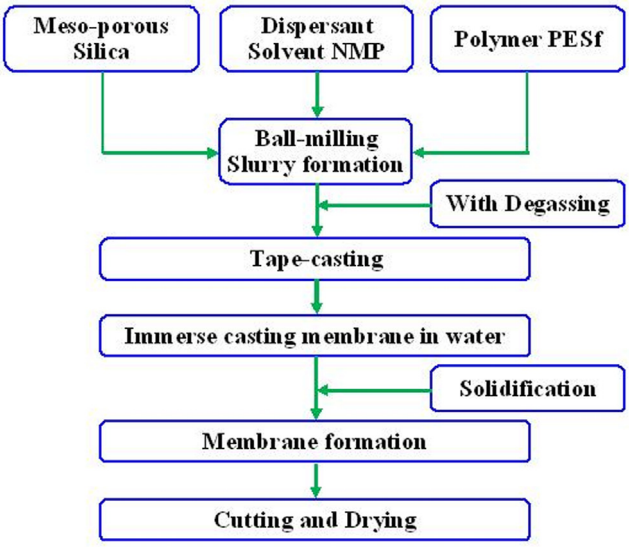

Fig. 2. Flow chart of tape-casting and phase inversion process for pristine MCM-41 membranes.

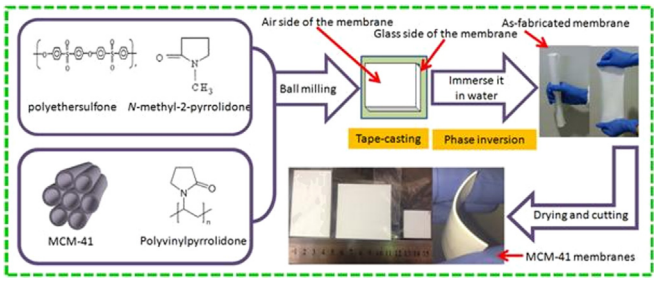

Fig. 3. Schematic drawing of tape-casting and phase inversion process for pristine MCM-41 membranes.

determination of the tensile strength and the ultimate elongation of tested membranes.

The tensile strength was calculated using Eq. (1):

$$\sigma_t = \frac{p}{bd} \tag{1}$$

where σ_t is the tensile strength (MPa), p is the maximum Load (N), b is the width (mm) of specimen and d is the thickness (mm) of specimen.

Ultimate elongation of the composite membrane was calculated using Eq. (2):

$$\varepsilon_t = \frac{L - L_0}{L_0} \times 100\% \tag{2}$$

where ε_t is the ultimate elongation (%), L_0 is the gauge length (mm) of the membrane and L is the maximum gauge length (mm) after the sample was stretched.

The pure water/methanol uptake test was carried out according to the following procedure: ten xMCM-41-m ($55 \le x \le 75$) membranes were first vacuum-dried at 100 °C overnight and weighted until a constant weight was obtained. The dried membrane (W_{dry}) was then soaked in deionized water/methanol for 24 h at 80 °C. Subsequently, the membranes were taken out and weighed (W_{wet}) using a microbalance after blotted dry with filtration paper. The water/methanol uptake was calculated using Eq. (3):

$$W_{H_2O/CH_3OH} = \frac{W_{wet} - W_{dry}}{W_{dry}} \times 100\% \tag{3}$$

where W_{wet} and W_{dry} represent the weight of the wet and dry membranes, respectively.

Swelling ratio of the composite membrane was calculated using Eq. (4):

$$S_{H_2O/CH_3OH} = \frac{A_{wet} - A_{dry}}{A_{dry}} \times 100\% \tag{4}$$

where A_{wet} and A_{dry} are the areas of the wet and dry membrane, respectively.

Thermogravimetric analysis (TGA) and derivative thermogravimetry (DTG) of PESf, HPW, xMCM-41–yHPW-m ($55 \le x \le 75$, $0 \le y \le 100$) composite membranes were conducted on a 2950 thermal analyzer (TA Instruments Inc., New Castle, DE) by heating the samples from room temperature to 700 °C with a heating rate of 10 °C min^{-1} under N_2 flow rate of 60 mL min^{-1}.

2.5. Conductivity and cell performance measurements

The proton conductivity of the xMCM-41–yHPW-m ($55 \le x \le 75$, $0 \le y \le 100$) composite membranes was measured with impedance spectroscopy using a Solartron 1260 frequency response analyzer in conjunction with a 1287 electrochemical interface at a frequency range of 1 Hz to 1 MHz with the signal amplitude of 10 mV under open circuit and the temperature range of 25–90 °C under 100% relative humidity (RH). The proton conductivity was calculated according to Eq. (5):

$$\sigma = \frac{L}{RA} \tag{5}$$

where σ represents the proton conductivity of membranes, L represents the thickness of membrane, R and A represent the membrane resistance and the area of membrane, respectively.

The xMCM-41–yHPW-m ($55 \le x \le 75$, $0 \le y \le 100$) mesoporous silica composite membrane was sandwiched between anode (direct methanol fuel cell anode, product code: 45374, Johnson Matthey, PtRu loading is 3.9 mg cm^{-2}) and cathode (direct methanol fuel cell cathode, product code: 45375, Johnson Matthey, Pt loading is 3.7 mg cm^{-2}) with diffusion layers. The active electrode area is 4 cm^2. Then the sandwiched structure was clamped and

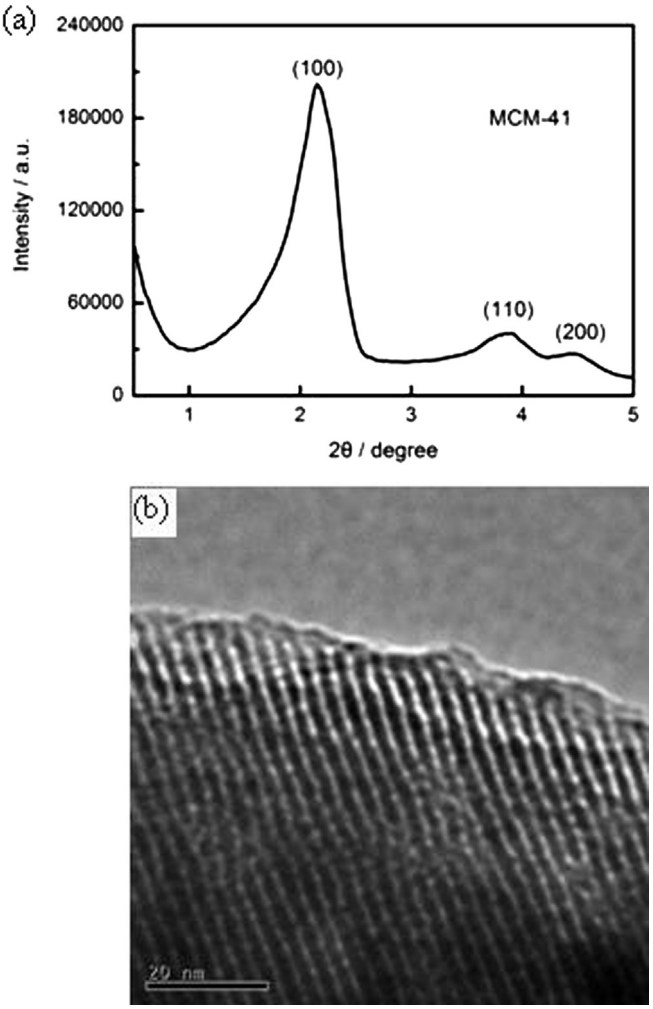

Fig. 4. (a) Small-angle X-ray scattering (SAXS) patterns and (b) TEM image of mesoporous silica MCM-41 powder.

sealed between two graphite plates with engraved flow field that were used for the membrane electrode assembly (MEA) characterization. The flow rate of H_2 was 100 mL min^{-1} and the flow rate of methanol solution (2 mol L^{-1}) was 1 mL min^{-1}, while dry air flow rate was fixed at 300 mL min^{-1}. The cell performance measurements were carried out from 90 °C to 150 °C. The conductivity of membranes was measured at different temperatures in the same set-up with carbon paper (Toray TGPH-060).

3. Results and discussion

3.1. SAXS and TEM of MCM-41

Fig. 4a shows the SAXS patterns of mesoporous silica MCM-41. As shown in Fig. 4a, there is an intense diffraction (100) peak along with two weak peaks assignable to (110) and (200), which is a typical diffraction pattern of mesoporous silica MCM-41 materials [35,38]. As shown in Fig. 4b, the transmission electron microscopy (TEM) image of mesoporous silica MCM-41 illustrates the regular hexagonal array of mesoporous channels, which further confirms that the synthesized sample has a 2D hexagonal structure with order of mesoscopic length scale and well-defined pore geometry.

3.2. Morphology of the MCM-41 membranes

Fig. 5 shows FESEM micrographs of the 55MCM-41-m membrane at different positions. The thickness of the membrane is ~350 μm as shown in Fig. 5b. Both microporous layer and macroporous layer have been formed during the solidification process (see Fig. 5a and c), which may be attributed to the different precipitation rates of NMP occurring within the nascent membranes [39,40]. The difference in precipitation rates occurred during the phase inversion stage where the exposed surface of the membrane contacted with large quantities of coagulant (tap water) faster than the other side of the membrane that was in contact with glass plate. The rapid precipitation occurred on the exposed surface leads to the formation of microporous structure, while the slower precipitation on the other side leads to macro voids [40–42]. Therefore, one side of the surface is more porous than the other side of the MCM-41 membranes. In addition, it also can be seen that the MCM-41 particles are well dispersed and connected to each other by the polymer network structure.

3.3. Tensile strength test

Good tensile strength and ductility are necessary in the application of proton exchange membranes. In order to investigate the mechanical properties of the MCM-41 membranes, tensile strength tests were conducted and the results are shown in Fig. 6. The tensile strength of 55MCM-41-m, 60MCM-41-m, 65MCM-41-m, 70MCM-41-m and 75MCM-41-m is 1.52 MPa, 1.02 MPa, 0.59 MPa, 0.30 MPa and 0.23 MPa with corresponding ultimate elongations of 10.24%, 9.42%, 8.25%, 4.72% and 3.50%, respectively. It is noted that the tensile strength and ultimate elongation for the MCM-41 membranes fabricated by tape-casting & phase inversion technique are lower than that of Nafion-117 and HPW incorporated to chitosan–hydroxy ethyl cellulose membrane that are used in direct methanol fuel cells [43], but slightly higher than for organic–inorganic composite membranes based on poly(vinylidene fluoride-co-chlorotrifluoroethylene)-graft-poly(styrene sulfonic acid) with embedded phosphotungstic acid [44]. It is obvious that both the tensile strength and ultimate elongation decreased almost linearly with the increased in mesoporous MCM-41 content. This may be attributed to the decrease of PESf content, which served as the cross-linked network of the membrane, thus, restricting the stretch of backbone and hindering the strain. The results concluded that

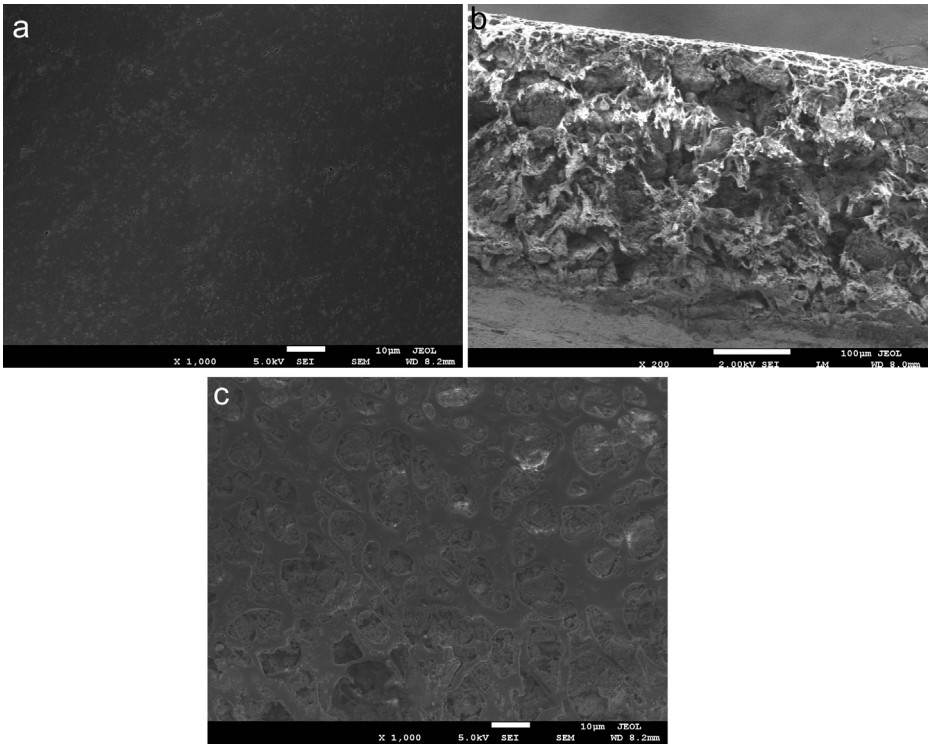

Fig. 5. FESEM morphologies of MCM-41 composite membrane fabricated by tape-casting & phase inversion technique: (a) surface microstructure of air side, (b) microstructure of cross section and (c) surface microstructure of glass side.

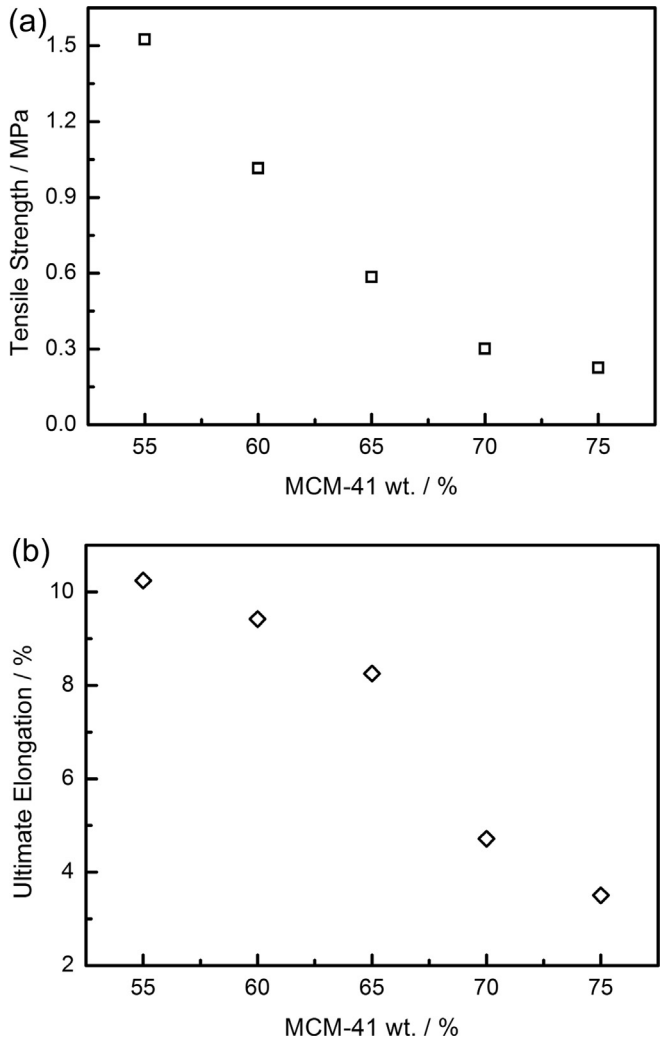

Fig. 6. (a) Tensile strength and (b) ultimate elongation of MCM-41 membranes as a function of MCM-41 content.

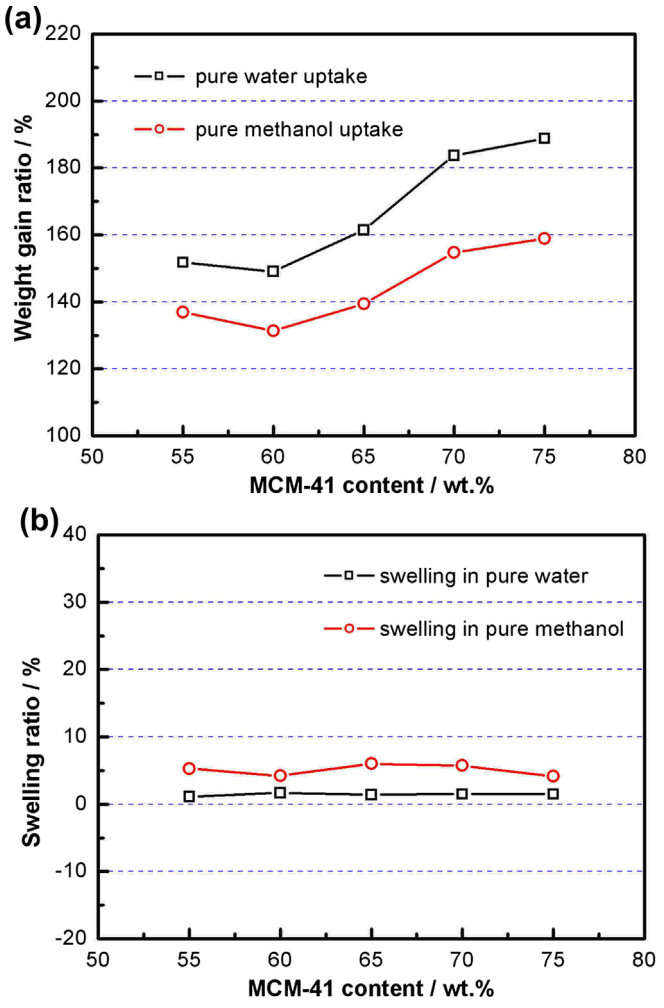

Fig. 7. The (a) weight-gain ratio and (b) swelling ratio of MCM-41 series membranes fabricated by gel casting technique as a function of solid state loading, and (c) weight-gain ratio of MCM-41–HPW-m series membranes as a function of HPW loading in pure water/methanol at 80 °C.

the mechanical properties of the MCM-41 membranes fabricated by tape-casting & phase inversion technique are mainly affected by the content of PESf.

3.4. Water/methanol uptake and swelling

Water content in the fuel cell is important because it affects the proton conductivity and mechanical stability of PEMs [45–49]. Generally, protons can be transported along with hydrogen-bonded ionic channels and hydronium ions such as H_3O^+ or $H_5O_2^+$ in the water. Hence, proton exchange membranes should absorb sufficient water. However, excessive water absorption will result in excessive swelling and loss of the dimensional stability. Therefore, it is important to control the amount of water uptake in the proton exchange membranes [49]. Fig. 7 shows the uptake and swelling ratio for composite membranes as a function of MCM-41 content in deionised water and methanol at 80 °C for 24 h. It can be seen in Fig. 7a that the water uptake of MCM-41 membranes increases with the content of MCM-41, and reaches ~190% (relative to the dry membrane) when MCM-41 loading was 75 wt.%. The increase in water uptake can be attributed to the water retention of the incorporated silica, which is due to the hydrogen bonding of H_2O molecules with the SiOH groups on the surface of synthesized MCM-41 powders (surface area: ~1000 $m^2\ g^{-1}$) [48]. On the contrary, the water uptake of MCM-41 composite membranes fabricated by gel-casting decreases with the increase in solid state loading (i.e. the MCM-41 content) of the formulated slurry [22]. Some factors that might have affected the water uptake of these two hybrid membranes: (i) poly(acrylic acid) is hydrophilic and weak acid, but PESf is hydrophobic and neutral. (ii) The silanols on the MCM-41 surface react with poly(acrylic acid) and restrict polymer chain mobility and free volume, which leads to more rigid and compact structure in the hybrid membranes and hence decreases water uptake [47,49,50]. (iii) There are no interactions between PESf and silanols on the meso-porous silica surface that will not limit the space absorbed water molecule by MCM-41. From the results of water uptake, it can be concluded that the composite membrane fabricated by tape-casting & phase inversion can absorb more water at high MCM-41 content, which is beneficial for higher HPW loading [14,22].

During the fuel cell operation, the dimensional change of membranes may be caused by the operating temperature and water or hydrocarbon fuel uptake of the membrane. In order to investigate the dimensional stability of MCM-41 membranes fabricated by tape-casting & phase inversion technique, the swelling ratio of membranes was tested by immersing in the deionised water and

methanol at 80 °C for 24 h. As shown in Fig. 7b, the swelling ratio of MCM-41 membrane with different MCM-41 content, in water and in methanol, is quite small at ~1.5% and ~5%, respectively. These values are lower than that of MCM-41 composite membranes fabricated via the gel-casting technique [22]. This can be attributed to the cross-linked network formed by hydrophobic PESf that restricts the swelling. The results of the swelling ratio indicate that the dimensions of MCM-41 membranes synthesized by tape-casting and phase inversion technique would be stable for fuel cell application, especially when using methanol/ethanol as the fuel.

3.5. TGA and DTG

Typical thermogravimetric analysis (TGA) and derivative thermogravimetry (DTG) spectra of PESf, HPW, 60MCM-41-m and 60MCM-41–31HPW-m are presented in Fig. 8. As shown in Fig. 8a, the weight loss of PESf occurred in the temperature range of 434–640 °C. It roughly loses 55.14 wt.% of its original weight. This implies that the MCM-41 membrane using PESf as the main support can operate up to 200 °C without any problems.

Three weight loss stages at 40–113, 115–267 and 369–520 °C can be distinguished in the DTG spectra of HPW (Fig. 8b). The locations of the weight loss stages observed here are in agreement with the reported values [51–55]. These weight losses can be respectively attributed to the loss of physical absorbed water, the loss of crystal water from HPW hydrate, and the decomposition of the Keggin structure. As shown in Fig. 8b, the crystal water of HPW is approximately 3.22 wt.%.

Two-stage degradation behaviour for 60MCM-41-m is observed in Fig. 8c. The initial thermal degradation temperature of 60MCM-41-m up to 69 °C is attributed to the loss of the moisture absorbed from the air and the loss of the water in the channels of MCM-41 [35,51]. The second degradation temperature of 60MCM-41-m, around 551 °C, is due to the thermal degradation of the organic chains which is corresponding to the spectra of PESf.

As shown in Fig. 8d, 60MCM-41–31HPW-m exhibited three stages of degradation at 26–118, 122–158 and 267–561 °C. The reason for the initial thermal degradation is similar to that of 60MCM-41-m. The second weight loss of 60MCM-41–31HPW-m in the temperature range 122–158 °C is approximately 0.33 wt.%. This is due to the loss of crystal water from HPW hydrate which is not impregnated into the channels of MCM-41. As the content of HPW in 60MCM-41–31HPW-m is 31%, the theoretical weight loss percentage of crystal water from HPW hydrate should be ~1.00% (3.22% × 31%), which is significantly higher than 0.33% observed from 60MCM-41 to 31HPW-m. The results revealed that about two-thirds of HPW impregnated into composite membranes fabricated by tape-casting & phase inversion technique has been moved into the channel of MCM-41 silica. The third main degradation peak of 60MCM-41–31HPW-m appears at ~375 °C which is much lower than both that of HPW and of 60MCM-41-m. This can be attributed to the strong acidity of phosphotungstic acid (HPW) that may have decreased the thermal degradation temperature of PESf.

In summary, the TGA/DTG results indicate that *x*MCM-41–*y*HPW-m membranes fabricated by tape-casting & phase inversion technique can operate up to 200 °C without any problem.

3.6. Proton conductivities

The proton conductivity measurements of *x*MCM-41–*y*HPW-m composite membranes were performed by impedance spectroscopy over the frequency range of 1 Hz to 1 MHz with the signal amplitude of 10 mV in the temperature range of 25–90 °C under 100% RH. The results were the average of measurements on at least three different samples. Fig. 9a shows the proton conductivity of 60MCM-41–*y*HPW-m composite membranes as a function of HPW loading measured at different temperatures. In the case of 60MCM-41–10HPW-m membrane, the conductivity is 0.011 S cm^{-1} and 0.023 S cm^{-1} at 25 °C and 80 °C, respectively. The conductivity of HPW/MCM-41 composite membrane with ~10% HPW loading fabricated by gel-casting technique was 2.4 × 10^{-3} S cm^{-1} and 7.7 × 10^{-3} S cm^{-1} at 25 °C and 80 °C [22], respectively, which is significantly lower than that of 60MCM-41–10HPW-m with the nearly same HPW loading. While the reason for these differences in

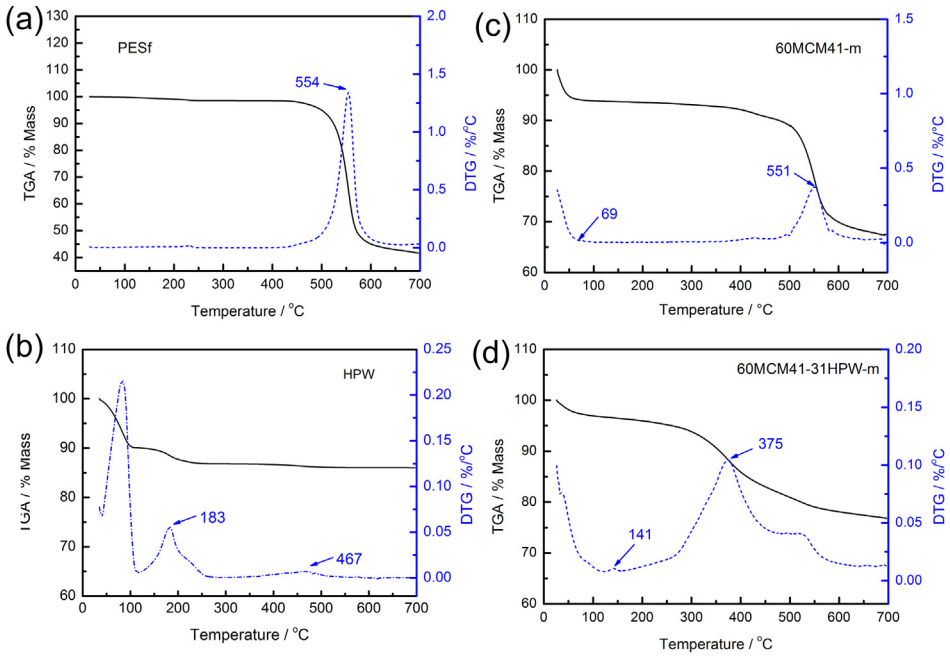

Fig. 8. Thermogravimetric analysis (TGA) and derivative thermogravimetry (DTG) curves of (a) PESf, (b) HPW, (c) 60MCM-41-m, (d) 60MCM-41–30HPW-m composite membranes measured from room temperature up to 700 °C.

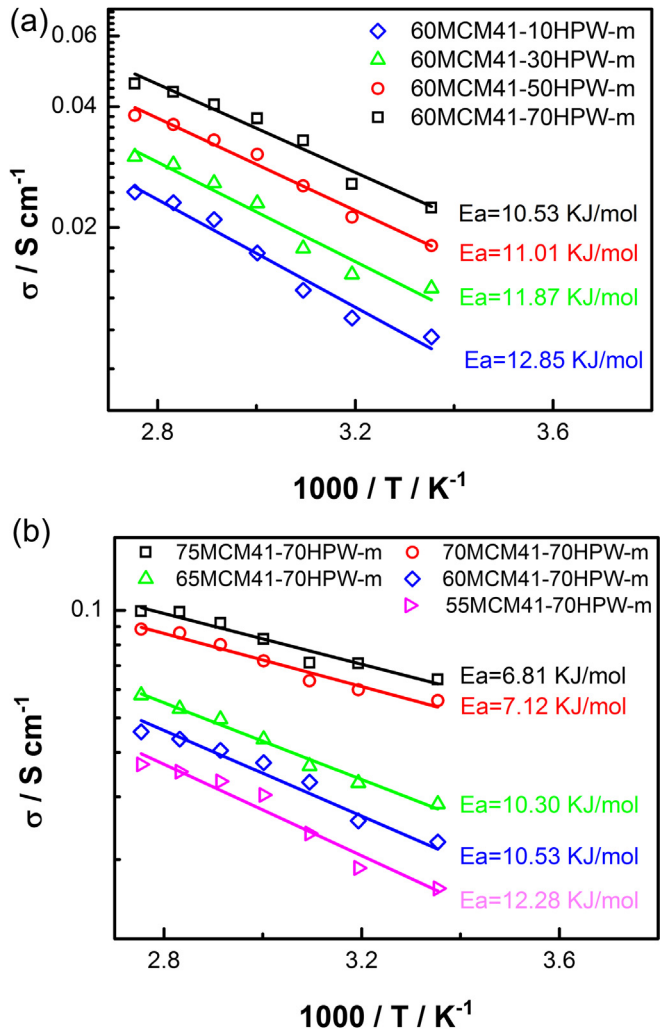

Fig. 9. (a) Conductivity of MCM-41–HPW-m series membranes fabricated by tape-casting & phase inversion technique as a function of HPW loading and a function of test temperature, (b) conductivity of *x*MCM-41–70HPW-m membranes as a function of MCM-41 content and a function of test temperature.

proton conductivity is not completely understood yet, the proton conductivity of the membranes has been significantly improved with further increase of HPW loading. In the case of 60MCM-41–70HPW-m, the conductivity was 0.044 S cm^{-1} at 80 °C, which is ~2 times higher than 0.023 S cm^{-1} measured on 60MCM-41–10HPW-m at 80 °C. The activation energies of the HPW/MCM-41 composite membranes with HPW loading of 10%, 30%, 50% and 70% are 12.85, 11.87, 11.01 and 10.53 kJ mol^{-1}, respectively, which are comparable with the reported results [22].

Densification and the micro-structural optimization of conductive materials are also critical in determining the proton conductivity properties of the electrolyte in fuel cells [29,30]. The conductivities of HPW/MCM-41 composite membranes fabricated by gel-casting technique are found to increase with the increase in solid state loading (i.e. increase in MCM-41 content) [22]. The proton conductivities of HPW/MCM-41 composite membranes as a function of MCM-41 content measured at different temperatures are shown in Fig. 9b. As shown in Fig. 9b, the proton conductivity of HPW/MCM-41 membranes fabricated by tape-casting & phase inversion increases from 0.035 S cm^{-1} to 0.098 S cm^{-1} when the MCM-41 content was increased from 55 wt.% to 75 wt.%. However, it is observed that it is difficult to further increase the MCM-41 content of the membrane. The excessive MCM-41 powder would be suspended into water during the solidification process, when more MCM-41 powder is added into the slurry. This can be attributed to the MCM-41 content in 75MCM-41-m where the limitation of PESf to form the organic three dimensional networks to hold further MCM-41 powder has been reached.

3.7. Single cell performance

To demonstrate the applicability of the HPW/MCM-41 composite membranes as a high-temperature proton-conductive electrolyte membrane, a single cell was assembled with a *x*MCM-41–70HPW-m ($55 \leq x \leq 75$) with thickness ca. ~0.35 mm by using PtRu/C catalyst in the anode and Pt/C catalyst in the cathode. The effective area of the cell was 4 cm^2. Fig. 10 shows the cell polarization performance as a function of MCM-41 content measured at 90 °C without external humidification in H_2/air and the performance of cell assembled from 75MCM-41 to 70HPW-m measured from 100 °C to 150 °C in methanol/air without external humidification. As shown in Fig. 10a, the open circuit voltage (OCV) of the cell using 55MCM-41–70HPW-m as electrolyte membrane is 0.93 V, comparable to 0.97 V at 100 °C reported by Lu et al. [14]. However, the OCV decreased from 0.93 V to 0.68 V when the MCM-41 content of the electrolyte membrane was increased from 55 wt.% to 75 wt.%, respectively, which indicated that the additional

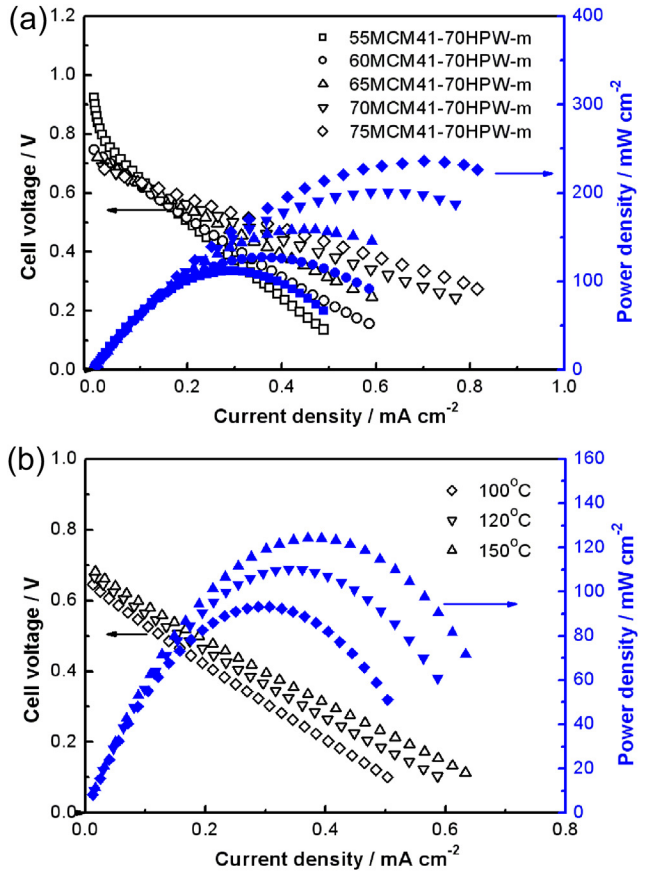

Fig. 10. (a) Polarization curves and power performance of a single cell with HPW/MCM-41 electrolyte membrane as a function of MCM-41 content in H_2/air without external humidification at 90 °C, (b) Polarization curves and power density of a single cell with a 75MCM-41–70HPW-m electrolyte membrane in methanol/air measured from 100 °C to 150 °C. Air flow rate: 300 mL min^{-1}; H_2 flow rate: 100 mL min^{-1}. Methanol solution (2 mol L^{-1}) flow rate: 1 mL min^{-1}. The membrane thickness was 0.35 mm.

MCM-41 silica phase did not contribute to higher OCV. The maximum output power density of the cell assembled from 75MCM-41 to 70HPW-m membrane is ~230 mW cm^{-2} at 90 °C, higher than the other cells assembled from composite membranes compared to the other membranes with different MCM-41 content. As shown in Fig. 10b, the maximum power output is 93 mW cm^{-2} and 125 mW cm^{-2} at 100 °C and 150 °C, respectively. This is significantly higher than 38 mW cm^{-2} and 90 mW cm^{-2} reported by Lu et al. [14], which is due to the lower membrane thickness (0.35 mm) of 75MCM-41–70HPW-m, compared to the membrane (0.8 mm) used by Lu et al. Clearly, the performance of HPW/MCM-41 mesoporous silica composite membrane cells can be improved by reduction of the thickness of the electrolyte membrane.

In summary, this study indicated that the HPW/MCM-41 composite membrane can be used as an effective proton-conductive electrolyte membrane for elevated-temperature PEMFCs.

4. Conclusions

The tape-casting & phase inversion and vacuum assisted impregnation process have been successfully applied to fabricate HPW/MCM-41 composite membranes. The preliminary results demonstrated that this process can be scaled up for the fabrication of large size HPW/MCM-41 composite membranes used in high-temperature PEMFCs. The results showed that large amount of loaded HPW is anchored in the mesoporous silica matrix, forming effective proton conduction pathways. The TGA curve of PESf demonstrated the thermal stability of MCM-41 membrane, which uses PESf as the main supporting network. The TGA result supported the notion that the MCM-41 membrane can operate below 200 °C without any problems. The proton conductivity result shows that the HPW/MCM-41 composite membrane has a high conductivity of 0.064 and 0.098 S cm^{-1} at 25 and 90 °C, respectively, with low activation energy of ca. 6.81 kJ mol^{-1}. Single cell performance test based on 75MCM-41–70HPW-m produced a peak power density of ~230 mW at 90 °C in H_2/air and 125 mW cm^{-2} at 150 °C in methanol/air without external humidification. The results demonstrated that the HPW/MCM-41 composite membrane can be used as an effective proton-conductive electrolyte membrane for elevated-temperature PEMFCs.

References

[1] U. Beuscher, S.J.C. Cleghorn, W.B. Johnson, Int. J. Energy Res. 29 (2005) 1103–1112.
[2] J.H. Wee, Renew. Sustain. Energy Rev. 11 (2007) 1720–1738.
[3] P. Agnolucci, Int. J. Hydrogen Energy 32 (2007) 4306–4318.
[4] M.Z. Jacobson, W.G. Colella, D.M. Golden, Science 308 (2005) 1901–1905.
[5] W.G. Colella, M.Z. Jacobson, D.M. Golden, J. Power Sources 150 (2005) 150–181.
[6] G.M. An, P. Yu, L.Q. Mao, Z.Y. Sun, Z.M. Liu, S.D. Miao, Z.J. Miao, K.L. Ding, Carbon 45 (2007) 536–542.
[7] B.C.H. Steele, J. Mater. Sci. 36 (2001) 1053–1068.
[8] D. Conolly, W. Gresham, US Patent 3282875, 1966, DuPont.
[9] C. Yang, P. Costamagna, S. Srinivasan, J. Benziger, A.B. Bocarsly, J. Power Sources 103 (2001) 1–9.
[10] J.L. Zhang, Z. Xie, J.J. Zhang, Y.H. Tanga, C.J. Song, T. Navessin, Z.Q. Shi, D.T. Song, H.J. Wang, D.P. Wilkinson, Z.S. Liu, S. Holdcroft, J. Power Sources 160 (2006) 872–891.
[11] T.A. Zawodzinski, T.E. Springer, J. Davey, R. Jestel, C. Lopez, J. Valerio, S. Gottesfeld, J. Electrochem. Soc. 140 (1993) 1981–1985.
[12] M.A. Hickner, H. Ghassemi, Y.S. Kim, B.R. Einsla, J.E. McGrath, Chem. Rev. 104 (2004) 4587–4611.
[13] X.M. Yan, P. Mei, Y.Z. Mi, L. Gao, S.X. Qin, Electrochem. Commun. 11 (2009) 71–74.
[14] S.F. Lu, D.L. Wang, S.P. Jiang, Y. Xiang, J.L. Lu, J. Zeng, Adv. Mater. 22 (2010) 971–976.
[15] P. Staiti, M. Minutoli, S. Hocevar, J. Power Sources 90 (2000) 231–235.
[16] O. Paschos, J. Kunze, U. Stimming, F. Maglia, J. Phys. Condens. Matter 23 (2011) 1–26.
[17] X.L. Chen, C.S. Wang, E.A. Payzant, C.R. Xia, D. Chu, J. Electrochem. Soc. 155 (2008) B1264–B1269.
[18] P. Heo, N. Kajiyama, K. Kobayashi, M. Nagao, M. Sano, T. Hibino, Electrochem. Solid-State Lett. 11 (2008) B91–B95.
[19] D.E. Katsoulis, Chem. Rev. 98 (1998) 359–387.
[20] H.L. Tang, M. Pan, S.P. Jiang, Dalton Trans. 40 (2011) 5220–5227.
[21] H.L. Tang, M. Pan, S.F. Lu, J.L. Lu, S.P. Jiang, Chem. Commun. 46 (2010) 4351–4353.
[22] L. Zhang, H.Q. He, R.K.S./O. Abdul Rasheed, W.J. Zhou, Y.H. Xue, O.L. Ding, S.H. Chan, J. Power Sources 221 (2013) 318–327.
[23] M.A. Janney, O.O. Omatete, C.A. Walls, S.D. Nunn, R.J. Ogle, G. Westmoreland, J. Am. Ceram. Soc. 81 (1998) 581–591.
[24] L. Zhang, S.P. Jiang, W. Wang, Y.J. Zhang, J. Power Sources 170 (2007) 55–60.
[25] L. Zhang, Y.J. Zhang, Y.D. Zhen, S.P. Jiang, J. Am. Ceram. Soc. 90 (2007) 1406–1411.
[26] L. Zhang, S.P. Jiang, C.S. Cheng, Y.J. Zhang, J. Electrochem. Soc. 154 (2007) B577–B582.
[27] S.P. Jiang, L. Zhang, Y.J. Zhang, J. Mater. Chem. 17 (2007) 2627–2635.
[28] C.S. Cheng, L. Zhang, Y.J. Zhang, S.P. Jiang, Solid State Ionics 179 (2008) 282–289.
[29] S.P. Jiang, L. Zhang, H.Q. He, R.K. Yap, Y. Xiang, J. Power Sources 189 (2009) 972–981.
[30] L. Zhang, H.Q. He, H.W. Wu, C.Z. Li, S.P. Jiang, Int. J. Hydrogen Energy 36 (2011) 6862–6874.
[31] S.P. Jiang, J. Power Sources 183 (2008) 595–599.
[32] C.J. Fu, S.H. Chan, Q.L. Liu, X.M. Ge, G. Pasciak, Int. J. Hydrogen Energy 35 (2010) 301–307.
[33] H. Moon, S.D. Kim, S.H. Hyun, H.S. Kim, Int. J. Hydrogen Energy 33 (2008) 1758–1768.
[34] A.K. Maiti, B. Rajender, Mater. Sci. Eng. A – Struct. Mater. 333 (2002) 35–40.
[35] J.S. Beck, J.C. Vartuli, W.J. Roth, M.E. Leonowicz, C.T. Kresge, K.D. Schmitt, C.T.W. Chu, D.H. Olson, E.W. Sheppard, J. Am. Chem. Soc. 114 (1992) 10834–10843.
[36] A. Corma, A. Martinez, V. MartinezSoria, J. Catal. 169 (1997) 480–489.
[37] S. Kawi, S.C. Shen, in: S. Abdelhamid, J. Mietek (Eds.), Studies in Surface Science and Catalysis, Elsevier, Alberta, 2000, pp. 227–234.
[38] S.M. Jin, G.Z. Qiu, F. Xiao, Y. Chang, C.F. Wan, M. Yang, J. Am. Ceram. Soc. 90 (2007) 957–961.
[39] X. Tan, Y. Liu, K. Li, Ind. Eng. Chem. Res. 44 (2004) 61–66.
[40] Z.G. Wang, N.T. Yang, B. Meng, X.Y. Tan, K. Li, Ind. Eng. Chem. Res. 48 (2009) 510–516.
[41] S. Mok, D.J. Worsfold, A.E. Fouda, T. Matsuura, S. Wang, K. Chan, J. Membr. Sci. 100 (1995) 183–192.
[42] T.H. Young, L.W. Chen, Desalination 103 (1995) 233–247.
[43] S. Mohanapriya, S.D. Bhat, A.K. Sahu, S. Pitchumani, P. Sridhar, A.K. Shukla, Energy Environ. Sci. 2 (2009) 1210–1216.
[44] D.K. Roh, J.T. Park, J.H. Koh, J.K. Koh, J.H. Kim, Ionics 15 (2009) 439–444.
[45] R.C. Jiang, H.R. Kunz, J.M. Fenton, J. Membr. Sci. 272 (2006) 116–124.
[46] Q. Deng, R.B. Moore, K.A. Mauritz, Chem. Mater. 7 (1995) 2259–2268.
[47] Q. Deng, R.B. Moore, K.A. Mauritz, J. Appl. Polym. Sci. 68 (1998) 747–763.
[48] C.C. Chen, H.Y. Tsi, W.C. Tsen, F.S. Chuang, S.C. Jang, Y.C. Shu, S. Wen, C.L. Gong, J. Appl. Polym. Sci. 123 (2012) 1184–1192.
[49] S.L. Zhong, X.J. Cui, S. Dou, Y.Q. Luo, W. Cui, S.J. Zhao, H. Zhu, W.C. Liu, Solid State Ionics 181 (2010) 1499–1504.
[50] C.W. Lin, R. Thangamuthu, C.J. Yang, J. Membr. Sci. 253 (2005) 23–31.
[51] Y. Liu, L. Xu, B.B. Xu, Z.K. Li, L.P. Jia, W.H. Guo, J. Mol. Catal. A: Chem. 297 (2009) 86–92.
[52] G. Kamalakar, K. Komura, Y. Sugi, Appl. Catal. A – Gen. 310 (2006) 155–163.
[53] G. Kamalakar, K. Komura, Y. Kubota, Y. Sugi, J. Chem. Technol. Biotechnol. 81 (2006) 981–988.
[54] J. Kaur, K. Griffin, B. Harrison, I.V. Kozhevnikov, J. Catal. 208 (2002) 448–455.
[55] I.V. Kozhevnikov, Chem. Rev. 98 (1998) 171–198.